

Microstructure of the surfactantlike effect in Ni/Ag(100) and (111)

Jean-Marc Roussel, Andrés Saúl, and Guy Tréglia
 CRMC2-CNRS, Campus de Luminy, Case 913, 13288 Marseille Cedex 9, France

Bernard Legrand
 SRMP/DECM, CEA Saclay, 91191 Gif-sur-Yvette Cedex, France
 (Received 20 December 1996)

Recent experiments on Ni/Ag systems have shown that the growth mode can be a floating monosubstrate or bisubstrate layer burying the deposited film. We study this surfactant effect by both mean-field and Monte Carlo kinetic approaches. The kinetic tight-binding Ising model in mean-field approximation gives quasisteady profiles consistent with local equilibrium concepts. In this framework, we find two and one capping Ag monolayers for Ag(100) and Ag(111), respectively, on a mostly pure Ni monolayer. Monte Carlo simulations reveal that this Ni “sandwich” structure is in fact made of embedded Ni precipitates with low interface energy regular polyhedra shapes. The cluster distribution is found to be larger for the less compact surface [i.e., (100)] and to obey the “Ostwald ripening” law. [S0163-1829(97)01116-8]

I. INTRODUCTION

The study of metal film deposited on a metal substrate, which has considerably developed with the appearance of the near-field microscopy, has shown a large variety of structural behaviors. If experiments are performed at an intermediate temperature giving rise to an interdiffusion limited to some planes close to the surface then a metastable surface alloy may be formed during the kinetics of dissolution.¹ When the corresponding bulk alloy of the two elements (deposit and substrate) has a tendency to form an ordered phase, the superficial compound is usually also ordered but could differ strongly from the equilibrium ones. On the other hand, when the type of chemical bonding of the atomic species is preferentially homoatomic (phase separation case), one observes two distinct situations depending on the tendency of the deposit element to segregate or not at the surface. In the first case, the deposited monolayers remain at the surface and may give rise to a layer-by-layer dissolution at the interphase.² In the second case, the kinetics may reveal a “surfactantlike” behavior that consists of the climb of substrate elements (B) through the deposit (A) to the surface.³ Thus, the A deposit layers can be buried below some B floating monolayers and can then persist during the growth or the dissolution.^{4–16}

Many ingredients can be responsible for these clearly non-Fickian dissolution modes. Apart from the temperature and the surface orientation of the substrate one has to take into account a possible size mismatch between the two constituents, the difference in surface energies, and the tendency of the alloy to either form ordered phases or to phase separate. Remembering that the equilibrium state of such a system is the complete dissolution of the deposit and therefore an infinitely dilute solid solution, it is necessary to use a kinetic model consistent with the thermodynamic equilibrium near the surface and containing the driving forces mentioned above. In this sense, from mean-field models to Monte Carlo simulations, different degrees of approximations have

been proposed to describe local order in these surface phenomena.

Auger spectroscopy results have shown that a deposit of one Ni monolayer on Ag(100) at room temperature leads, after an annealing at 620 K, to the formation of an Ag bilayer burying the Ni atoms.³ Many other cases showing this “surfactantlike” effect have been found for systems such as Rh/Ag,^{6–8} Cr/Ag,⁹ Fe/Ag,¹⁰ Co/Cu,^{11,12} Fe/Cu,¹³ Ni/Cu,¹⁴ Pt/Au,¹⁵ and Fe/Au,¹⁶ which present a strong tendency to phase separation and a significant difference between the two components’ surface energies favoring the substrate segregation.

The purpose of the present work is to investigate the dissolution modes of 1 ML Ni/Ag as a function of the crystallographic orientation of the substrate: (100) and (111). This paper is organized as follows: in Sec. II, we formulate the kinetic tight-binding Ising model (KT BIM), after a brief sketch of its origin.^{17–20} The homogeneous mean-field approximation used in the KT BIM prevents the study of both the nucleation phenomena and microstructure shapes occurring during surface phase transition. Therefore, to go beyond this average method we employ a kinetic Monte Carlo algorithm based on the same energetic model. In Sec. III, we present the results of simulation of 1 Ni ML on Ag(100) and (111) at 620 K using the two methods mentioned above. Both approaches predict the occurrence of a quasisteady Ni sandwich structure during the kinetics of dissolution. The Monte Carlo simulation gives more detail concerning the local order of this structure and predicts the existence of embedded Ni clusters close to the surface. We discuss the shape, the mobility, and the size evolution of these clusters and consider the influence of the surface orientation on the coarsening sequences. Discussions and conclusions are given in Sec. IV.

II. THE NUMERICAL MODEL

Let us summarize the main aspects of the tight-binding Ising model (TBIM) developed to study equilibrium surface

segregation in concentrated transition and noble metal alloys A_cB_{1-c} . From the electronic structure of the disordered alloy one can derive an effective Ising Hamiltonian.^{17,18} The internal energy of the Ising model can be written as

$$H^{\text{TBIM}} = \sum_n p_n \left\{ \Delta h_n^{\text{eff}} + \Delta H_n^{\text{size}} - \sum_{m \neq n} V_{nm} \right\} + \sum_{n,m \neq n} p_n p_m V_{nm}, \quad (1)$$

where p_n is the spinlike occupation variable equal to 1 (0) if the site n is occupied by an atom A (B), and the following is true.

(i) V_{nm} is the effective pair interaction between atoms at sites n and m :

$$V_{nm} = \frac{1}{2} (V_{nm}^{AA} + V_{nm}^{BB} - 2V_{nm}^{AB}). \quad (2)$$

For fcc structures it is negligible beyond first neighbors. $V_{nm} = V$ if n, m are first neighbors and $V_{nm} = 0$ if they are not. The sign of V gives the tendency to order ($V > 0$) or phase separation ($V < 0$) of the system. When at least one site belongs to the surface, the interaction V is enhanced and is denoted by V_0 .

(ii) Δh_n^{eff} is generally different from zero only for the surface (and sometimes first underlayer) plane. In that case Δh_0^{eff} is very close to the difference in surface energies between the pure constituents.

(iii) ΔH_n^{size} accounts for a possible size effect; this term is calculated by means of tight-binding quenched molecular dynamics^{21–23} and is only significant close to the surface. In this scheme ΔH_0^{size} is calculated as the size-dependent part of the total energy involved when a single impurity is moved from the totally relaxed bulk to the totally relaxed surface.

This model has been used to study equilibrium segregation of binary alloys using either a mean-field^{23–25} description or a Monte Carlo one.²⁶

In the mean-field approximation for a binary alloy A_cB_{1-c} and in the presence of a surface, one usually defines i -plane concentrations c_i parallel to the surface ($i=0$: surface; $i=1$: first underlayer, etc.; $i=\infty$: bulk plane) in order that $\forall n \in (i\text{-plane}), c_n = \langle p_n \rangle = c_i$. This mean-field approximation, which neglects the short-range correlations, reduces the internal energy to a one-dimensional problem. The mean value of the grand-canonical free energy is $\langle G \rangle = \langle H^{\text{TBIM}} \rangle - T \langle S \rangle - \mu \langle N_A \rangle$ where $\langle H^{\text{TBIM}} \rangle$ is the mean value of the internal energy from Eq. (1), T is the temperature, $\langle S \rangle$ the mean value of the entropy calculated in Bragg Williams approximation, μ the chemical potential, and $\langle N_A \rangle$ the mean number of A atoms in the system. Its minimization ($dG/dc_i = 0, \forall i$) leads to the following system of coupled nonlinear equations:

$$\frac{c_i}{1-c_i} = \frac{c}{1-c} \exp \left\{ - \frac{\Delta H_i}{kT} \right\}; \quad (3)$$

here c is the bulk concentration, ΔH_i is the segregation enthalpy for the i plane, that is, the energy needed to exchange an atom B in the i plane by an atom A from the bulk:

TABLE I. Surface specific energetic parameters (in eV/atom) used in this work (see text) for the (100) and (111) surfaces of the Ag(Ni) system. Z and Z' are the numbers of first neighbors in the same and adjacent planes, respectively.

	Z	Z'	ΔH_0^{size}	Δh_0^{eff}	ΔH_1^{size}	Δh_1^{eff}
100	4	4	-0.04	0.39	-0.02	0
111	6	3	0	0.30	-0.02	0

$$\Delta H_0 = \Delta H_0^{\text{size}} + \Delta h_0^{\text{eff}} + V(Z + 2Z') - V_0(Z + Z') + 2Z(V_0c_0 - Vc) + 2Z'(V_0c_1 - 2Vc),$$

$$\Delta H_1 = \Delta H_1^{\text{size}} + \Delta h_1^{\text{eff}} + VZ' - V_0Z' + 2ZV(c_1 - c) + 2Z'(V_0c_0 + Vc_2 - 2Vc),$$

$$\Delta H_i = 2ZV(c_i - c) + 2Z'V(c_{i+1} + c_{i-1} - 2c). \quad (4)$$

Z and Z' are the numbers of first neighbors in the same and adjacent planes, respectively.

One can also use a Monte Carlo approach to study equilibrium by using, for example, the standard Metropolis algorithm:²⁷ rejecting and accepting configurations according to the internal energy given by the Ising Model [Eq. (1)].

For the $\text{Ag}_{1-c}\text{Ni}_c$ system the values in Table I are used²⁴ for the above-mentioned energetic quantities and the two surface orientations. The values of the effective pair interaction are $V = -0.053$ eV and $V_0 = 1.5$ V.

A. Mean-field kinetics

To be able to follow the kinetic path from a given initial condition, one can also use a simple one-dimensional model consistent with the equilibrium model. This kinetic extension of the TBIM [the KTBIM (Refs. 19 and 20)] also assumes homogeneous concentration per plane parallel to the surface and ensures that the steady-state concentration profile corresponds to the equilibrium profile given by Eq. (3). The time dependence of the mean concentration $c_i(t)$ is calculated as a detailed balance between incoming and outgoing fluxes:²⁸

$$\frac{\partial c_i}{\partial t} = \frac{D}{d^2} \left[(1-c_i) \left\{ \gamma_{i-1} c_{i-1} + \frac{c_{i+1}}{\gamma_i} \right\} - c_i \left\{ \frac{(1-c_{i-1})}{\gamma_{i-1}} + \gamma_i (1-c_{i+1}) \right\} \right], \quad (5)$$

where $D = D_0 \exp(-Q/kT)$ is the bulk diffusion constant and d the interplanar distance. γ_i is the transition probability for an exchange between an A atom in plane i and a B atom in plane $i+1$ and it is related to the instantaneous segregation energies:

$$\gamma_i(t) = \exp \left(\frac{\Delta H_i(t) - \Delta H_{i+1}(t)}{2kT} \right). \quad (6)$$

The dynamics of the system is found by iterating the system of Eqs. (5) using a constant time step algorithm. A large enough number of equations (N) is needed in order to get a dynamics independent of the system size. For the dissolution kinetics of k monolayers we start the simulation with the

initial condition $c_i(0)=1$ for $i=0,k-1$; $c_i(0)=0$ for $i=k,N$ and the boundary condition $c_{N+1}(t)=0$ in order to mimic a highly dilute volume.

Let us mention that, when all the energetic forces vanish in Eqs. (5), we recover the discrete version of the classical Fick's equation

$$\frac{\partial c_i}{\partial t} = \frac{1}{t_0}(c_{i+1} + c_{i-1} - 2c_i), \quad (7)$$

where $t_0 = d^2/D$.

For the $\text{Ag}_{1-c}\text{Ni}_c$ system the prefactor and activation energy for diffusion were taken from Ref. 29: $D_0 = 15 \text{ cm}^2/\text{s}$ and $Q = 2.256 \text{ eV}$.

B. Monte Carlo kinetics

A Monte Carlo realization of the kinetic process can be modeled using the standard Metropolis algorithm in conjunction with the energetics provided by the TBIM. By allowing exchanges only between first neighboring atoms, one can simulate an effective diffusion process and describe the dynamical evolution of the system. We are aware that such an algorithm should be inefficient when exchange probabilities are very small (low-temperature cases). The computing times being not too large for the simulations performed, we use the method that was discussed in more detail in a previous work.²⁶

We perform simulations in a system box of $(60 \times 60 \times 100)$ fcc unit cells with periodic boundary conditions in the directions parallel to the surface plane. In this way, we ensure that no size effect modifies the average values calculated in the following section. The initial condition simulates the experimental starting condition: a given number of full layers of (minority) Ni atoms are placed over a substrate of (majority) Ag atoms.

III. RESULTS

A. Mean-field results

Experimental results have shown that a deposit of one Ni monolayer on Ag(100) at room temperature leads, after annealing at 620 K, to the formation of an Ag bilayer burying the Ni deposit.³ This structure that is obtained after 10 min at $T = 620 \text{ K}$, does not evolve subsequently, at least in several hours, even if the thermodynamical equilibrium state is the complete dissolution. A previous KTBIM study³ in mean-field approximation of a very rapid deposit (flash) of one monolayer at room temperature followed by an annealing at 620 K led to an $\text{Ag}/\text{Ag}/\text{AgNi}/\text{AgNi}/\text{Ag}\cdots$ profile after 8 min, in very good agreement with the experimental results. It was estimated that this profile remains for more than one month before complete dissolution. Moreover, by using an extension of the KTBIM we have examined a possible competition between the incoming deposit flux of Ni and the climb of Ag. This study came to the conclusion that the depth and spatial extension of the buried film could depend strongly on the speed of the incoming flux.³⁰ Therefore, it is worth noticing that to avoid this flux dependence the following simulations correspond to the experimental initial conditions described before.

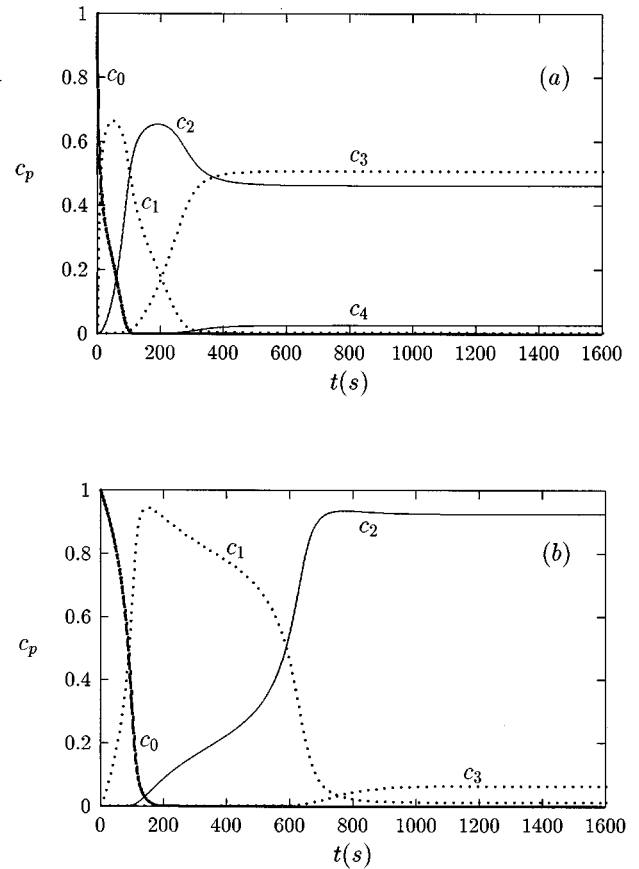


FIG. 1. Ni layer concentrations $c_p(t)$ vs time during the KTBIM dissolution of 1 Ni ML deposited on (a) Ag(100) and (b) Ag(111) substrates and annealed at $T = 620 \text{ K}$. $p = 0$: adsorbate layer, $p = 1$: substrate surface; $p = 2$: substrate first underlayer, etc.

The KTBIM kinetics of dissolution in the mean-field approximation of one Ni monolayer deposited on Ag(100) and (111) substrates at $T = 620 \text{ K}$ are shown in Fig. 1. In both cases, Ni almost instantaneously disappears from the surface but, instead of dissolving into the substrate (Fickian dissolution case), it occupies the third and fourth underlayers, forming a $\text{Ag}/\text{Ag}/\text{AgNi}/\text{AgNi}/\text{Ag}\cdots$ profile for (100) whereas it is confined in the third one ($\text{Ag}/\text{Ag}/\text{Ni}/\text{Ag}/\text{Ag}\cdots$ profile) for (111). The depth of two Ag monolayers capping the Ni monolayers differs from the results in Ref. 5 where a $\text{Ag}/\text{Ni}/\text{Ag}/\text{Ag}\cdots$ profile for Ni/Ag(100) was proposed. In our case it is easy to see that this difference is a consequence of the enhancement of the effective pair interaction at the surface.³ However, this single Ag capping monolayer has been also observed using our model for a Ni deposit beyond 1 ML and a particular range of incoming flux.³⁰

Notice that for both orientations, the kinetics reveal a not too strong time dependence for the occurrence of the metastable Ni buried monolayer: 10 min for (100) and 15 min for (111). For the (100) surface, most of the Ni matter crosses rapidly the first two surface planes. For the (111), the dissolution occurs in two steps, first the Ni monolayer comes down almost instantaneously from the surface to the first underplane and then migrates more slowly to form the above-mentioned quasisteady profile. The main difference is then that Ni spreads over two planes for (100) and one plane for (111).

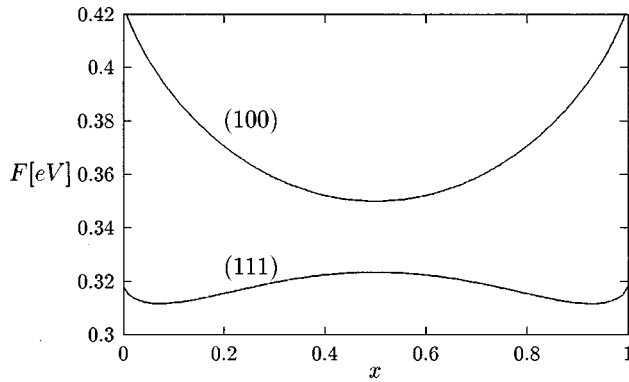


FIG. 2. Free energy of a $0/0/1-x/x/0/0$ profile, i.e., 1 Ni ML confined in the third and fourth (with concentration x) underlayers of Ag(100) and (111) substrates at $T=620$ K. The x values at the F minima correspond to the quasisteady $c_3(t)$ concentrations obtained kinetically in Fig. 1.

As long as the quantity of Ni can be considered as concentrated in the first four planes, we can use energetic arguments to understand these kinetic stabilizations (local equilibrium²⁵). If we consider that the 1 Ni ML is spread between the third and fourth layers, we can write the free energy of the system as depending on one parameter only, the Ni concentration in the fourth plane $c_2=1-x, c_3=x$:

$$F(x) = 2V[x(x-1)(Z-Z') - Z'] + 2kT[x \ln x + (1-x) \ln(1-x)] \quad (8)$$

In Fig. 2 we plot the free energy $F(x)$ versus x for both orientations. $F(x)$ presents only one minimum at $x=0.5$ for the (100) orientation and two minima at $x=0.935$ and $x=0.065$ for the (111) direction. These values of x for the free-energy minima are numerically equal to the quasisteady concentration of the third plane found kinetically.

One can wonder about the actual validity of this difference between the two orientations since the third or fourth layers can be considered as bulklike. One should then recover the same three-dimensional behavior in both cases. This is not true here; because of artifacts of the mean-field approximation, the separation between an interlayer (Z') and an intralayer (Z) number of neighbors is no longer relevant here.

B. Monte Carlo results

Strictly speaking, the mean-field approximation makes sense only in the limit of a long-range interaction or a very dilute situation and therefore it does not bring any local order information.

In Fig. 3 we show the Ni concentrations per plane versus time τ for the annealing of 1 Ni ML on Ag(100) and (111) at 620 K using the Monte Carlo method described in Sec. II 3. Starting from a full surface monolayer of Ni, we observe a rapid decrease of the Ni concentration of the surface and subsurface planes leading to two practically pure Ag capping monolayers. Then, the major difference with the previous mean-field case is that the Ni matter now expands among about 6–7 layers instead of only 1 or 2 (notice the change in

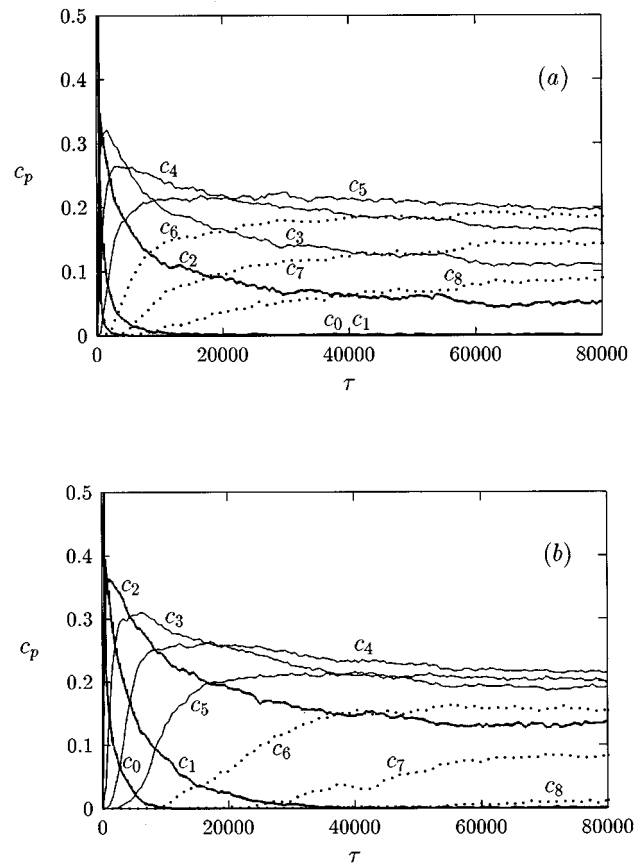


FIG. 3. Ni layer concentrations $c_p(\tau)$ vs time during the Monte Carlo dissolution of 1 Ni ML deposited on (a) Ag(100) and (b) Ag(111) substrates and annealed at $T=620$ K. $p=0$: adsorbate layer; $p=1$: substrate surface; $p=2$: substrate first underlayer, etc. The simulation box contains $60 \times 60 \times 100$ fcc unit cells for the (111) orientation and $84 \times 84 \times 100$ for the (100) one.

vertical scale between Figs. 1 and 3). By performing many random paths and for different box sizes, we ensure that the profiles (concentrations per plane) are identical and therefore correspond to the same quasisteady state. One can then wonder what is the structural arrangement of the Ni atoms when the same quantity of matter (1 ML) is spread over a larger depth. Figure 4 displays an example of microstructural evolution of a Monte Carlo simulated 1 ML Ni/Ag(111) during thermal annealing at 620 K at two different theoretical times before ($\tau \approx 2600$) and after ($\tau \approx 80000$) stabilization. Instead of forming a pure Ni monolayer parallel to the surface, the simulation gives rise to floating Ni clusters under some Ag pure surface planes. These observations lead us to formulate the following questions: What is the morphology of these buried Ni clusters with respect to the substrate orientation? What is the evolution of the number of clusters and of the cluster size distribution with time?

Concerning the first question, we observe pure Ni clusters presenting (111) and (100) facets (see Fig. 4). Such a picture is in agreement with equilibrium shapes of free fcc clusters.^{31,32} To get more insight, we report the configuration-dependent part of the interfacial energy of each cluster in a simple broken bond model, written as

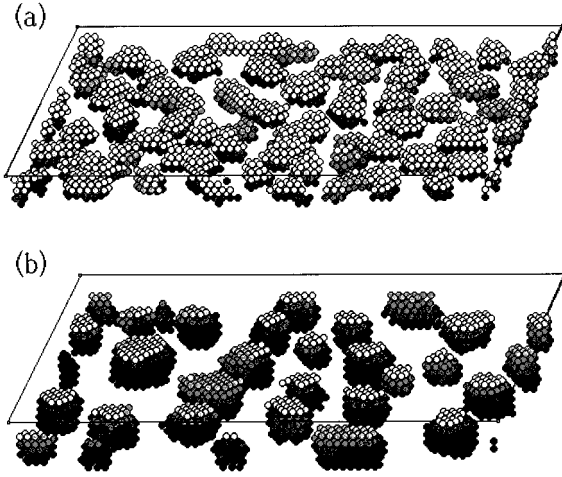


FIG. 4. Two snapshots from the Monte Carlo simulation of 1 Ni ML on Ag(111) at $T=620$ K: (a) before ($\tau=2600$) and (b) after ($\tau=80000$) the stabilization time. Only Ni atoms are shown and from the surface plane (white) to the eighth plane (dark grey), the grey scale color of the atoms represents the depth of the plane measured from the surface.

$$E_{\text{int}} = \sum_i \frac{Z_i}{Z + 2Z'}, \quad (9)$$

where i sums over all the atoms of the cluster and Z_i is the number of Ag first neighbors of the i th Ni atom. In Figs. 5(a) and 5(b), we plot the instantaneous interfacial energies of the clusters shown in Figs. 4(a) and 4(b) (corresponding to times before and after the stabilization, respectively) and we compare them with the interfacial energies of some regular fcc polyhedra.³¹ Figure 5(b) confirms then our observation since the Ni precipitate interfacial energies are very close to the cubo-octahedral and Wulff polyhedral energies, which are known to be the most stable atom arrangements in fcc structure. However, the thermal and kinetic fluctuations allow Ni clusters to take octahedral and dodecahedral shapes. The result is therefore a combination of these morphologies giving rise to buried Ni clusters presenting essentially (111) and (100) facets at the quasisteady state. Concerning the snapshot taken before the stabilization in Fig. 5(a), the main difference comes from the dispersion in energy values, which is larger due to a strong coagulation regime.

Let us now focus on the question of the time evolution of the number of clusters $n_c(\tau, l)$ and of the average cluster size $\langle s(\tau, l) \rangle$, where l is the lateral size of the simulation box. The number of clusters observed in one simulation for a given value of l does not have any physical meaning. At $\tau=0$ there is only one cluster, i.e., the deposited layer, then $n_c(0, l) = 1$ and $\langle s(0, l) \rangle = l^2$, the number of atoms in the surface of the simulation box [more precisely $l^2/2$ for the (100) orientation and l^2 for the (111) one]. For $\tau > 0$ the low solubility of Ni on Ag at this temperature prevents the diffusion of the Ni atoms into the bulk and therefore practically all the deposited atoms remain near the surface forming clusters. The average cluster size is in this case very close to the inverse of the number of clusters $\langle s(\tau, l) \rangle \approx l^2/n_c(\tau, l)$. Moreover we have found that, for $l \geq 60$, the number of clusters $n_c(\tau, l)$ at $\tau \geq 0$ is proportional to the number of depos-

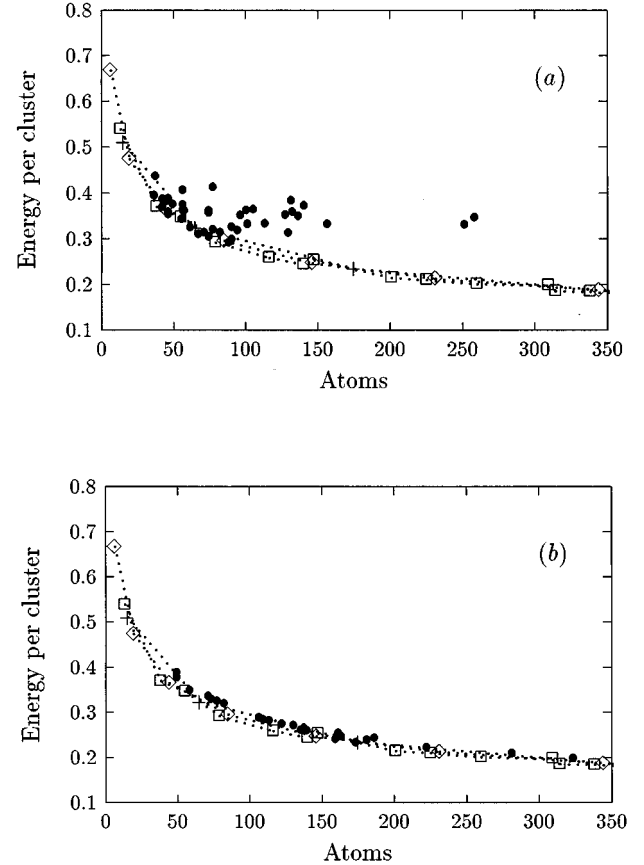


FIG. 5. Interfacial energies of the Ni clusters (●) shown in Fig. 4, (a) before ($\tau=2600$) and (b) after ($\tau=80000$) the stabilization time, compared to some regular fcc polyhedra: octahedron (◇), dodecahedron (+), and cubooctahedron (□). The cluster interfacial energies are calculated from Eq. (9) (see text).

ited atoms l^2 . It therefore implies the independence of the $\langle s(\tau, l) \rangle$ function with respect to l .

In Fig. 6 we show the average cluster size $\langle s(\tau) \rangle$ for both orientations. We observe identical features concerning the general evolution of the kinetics. After a practically instantaneous initial decrease of the number of Ni atoms per cluster, we see a rapid increase of the average volume $\langle s(\tau) \rangle$ and therefore a strong decrease of the cluster population. From this early stage of the dissolution it results that a considerable precipitate coagulation regime occurs, which confirms the preceding conclusion from Fig. 5(a). The main difference between the two orientation kinetics comes from the very beginning of the dissolution. Indeed, we notice the crucial influence of the surface orientation on the initial cluster population. At $\tau \approx 0$ the energy difference for one Ni atom to leave a full Ni surface monolayer is

$$\Delta E = -\Delta h_0^{\text{eff}} - \Delta H_0^{\text{size}} + \Delta H_1^{\text{size}} + \Delta h_1^{\text{eff}} + (2Z' - Z - 2)V_0 - (Z + Z')V, \quad (10)$$

which is positive for the (111) surface and negative for the (100), yielding at $T=620$ K a Metropolis exchange probability equal to 1 for the (100) orientation and 0.0026 for the (111). It leads to a cluster germ distribution greater for the

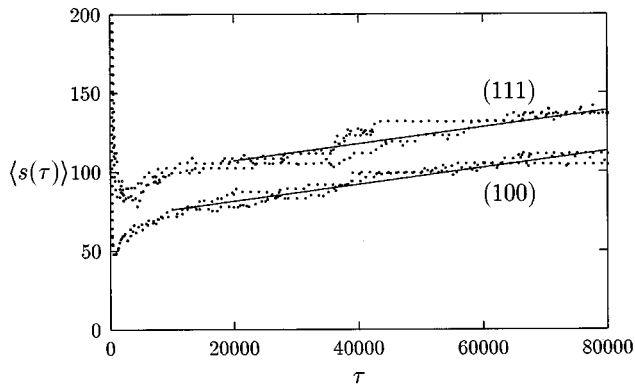


FIG. 6. Average cluster size $\langle s(\tau) \rangle$, in number of Ni atoms vs time (points) for two different Monte Carlo simulations and two surface orientations (100) and (111). The simulation box lateral size is $l=84$ for the (100) surface and $l=60$ for the (111) one. The solid lines are a guide for the eye only.

less compact surface (see Fig. 6). This difference remains during the kinetics since we found an average cluster size larger for the (111) substrate.

For larger time, at the quasisteady state, $\langle s(\tau) \rangle$ exhibits a linear growth with time. This stage can be interpreted in terms of ‘‘Ostwald ripening,’’ i.e., a coarsening regime where the interfacial energy is the only driving force and where the rate of development is governed by lattice diffusion. The system evolves in such a way as to minimize its interfacial area, the physical process being due to higher solubility of small particles (Gibbs-Thompson), which induces a solute flow from the smaller to the larger clusters. That phenomenon has been analyzed at various levels of sophistication, from a spherical precipitate description^{33–35} to a more extended theory taking into account volume fraction effects.³⁶ All these assumptions lead to a linear time dependence for the average cluster size in agreement with our results. The proportionality constant is predicted to increase when the concentration gradients around adjacent particles interplay,³⁶ which is our case according to concentrations per plane in Fig. 3.

IV. DISCUSSION AND CONCLUSION

We have shown here that a simple kinetic mean-field approach could bring valuable information for guiding Monte Carlo simulations. This assertion is verified for the dissolution of a very thin 1 Ni ML deposit on Ag. The KTBIM enables one to describe the general kinetic behaviors, in particular the depth and the time occurrence of the floating Ag bilayer. By performing kinetic Monte Carlo simulations we have deepened these points and we have shown that Ni clusters are confined in a few planes parallel to the surface under two Ag monolayers. We have seen a strong influence of the surface orientation on the number of germs explained by the different values of the initial exchange probabilities. Finally, we have found that the steady stage of the surface phase separation follows the predicted Ostwald ripening law for collective behavior of a precipitate population.

It should be noticed that some physical effects have not been taken into account in our simulations. In metallic al-

loys, the diffusion proceeds via vacancy jumps towards nearest-neighbor atoms. The process we have used is thus an effective exchange as a consequence of two vacancy-atom exchanges. A more realistic model would be to use a frequency of vacancy jumps in place of the effective exchange rate used in this work. This sophistication could favor exchange at the surface due to vacancy segregation and therefore modify the kinetics. However, the presence of the surface and the very small vacancy concentration at the temperature considered forbid a simple computing modification for taking into account this mechanism. This point is worth future study. Moreover, we are aware that the present model, which relies on a rigid lattice assumption, does not take into account in a proper way the atomic displacements due to the large size mismatch of about 14% between Ag and Ni. We also plan to focus on this effect in a future work. This requires one to derive potentials (i.e., from tight-binding or embedded-atom method) coupled with a kinetic Monte Carlo algorithm allowing atomic displacements. Details presented in this work should be also relevant for systems with negligible size mismatch, which present coherent precipitation as Ni/Cu (Ref. 14) or Co/Cu.^{11,12}

In summary, the main driving forces of this surfactant effect are unambiguously the surface energies of the two constituents. Both on experimental and theoretical sides the results converge to the evidence of this original growth mode. For the capping substrate overlayer a thickness of one or two atomic layers is reported for systems showing a great deal of analogy with the Ni/Ag system in terms of thermodynamic parameters. This concerns systems such as Rh/Ag,^{7,8} Ni/Cu,¹⁴ Co/Cu,^{11,12} and Pt/Au,¹⁵ which present a phase separation tendency, a size mismatch, and surface tension difference that do not retain the deposit at the surface and a fcc/fcc structure. For systems presenting the same sequence of energetic parameters but where only the crystal type of the deposit film differs, similar growth features have been also observed. This is the case for Fe/Cu,¹³ Fe/Ag,¹⁰ Cr/Ag,⁹ and Fe/Au,¹⁶ where the structure of the deposit film is bcc. Finally we emphasize that the surface enrichment by substrate atoms during the dissolution is not specific only to phase separation systems but can happen with some different features for systems with bulk order tendency,³⁷ e.g., Au/Ag.^{38,39}

If the surface enrichment is clearly due to the difference in surface energies, a large variety of geometries must exist for the encapsulated structure depending on the thickness of the initial deposit, on kinetic limitations related to the temperature, on the possible size mismatch, and on the tendency of the alloy to bulk order or not. Regarding the influence of deposit thickness and for a Ni/Ag-like system, we expect that a critical size should give rise to either a clustering as predicted in the present work (very thin deposit case) or a planar interphase as mentioned in experimental works^{6,11,12} (thick deposit case). Calculations are under way to check this assertion. The original Ni clustering under some Ag layers presented in this paper could be experimentally checked by grazing-x-ray analysis coupled with Auger characterization.⁴⁰

On the theoretical side, from *ab initio* calculations^{38,41} to semiempirical models,^{5,8} static simulations have brought out the energetic preference of a planar sandwich layer buried

under one or two substrate atomic layers compared to a planar surface adlayer. No other static morphologies have been simulated or considered to our knowledge and moreover we have seen here that a dynamical description of the dissolution is necessary to obtain the quasisteady profile. In Ref. 8, molecular dynamics is used within the corrected effective medium method for describing Rh penetration into the Ag substrate. The description of the first stage of the deposit migration has been possible. A more realistic simulation is still very demanding in computing time, which did not allow the authors to explore the dissolution until the kinetic meta-

stabilization. Recently (see Ref. 15) a molecular dynamics investigation of the early growth mode of Pt/Au(100) has been reported. It is found that the replacement mechanism appears in conjunction with a local corrugation of the reconstructed Au(100) substrate, which thus governs the very first stage of the incorporation. In order to be able to account for the actual atomic mechanisms (exchange, diffusion, vacancies) while following the complete dissolution, we plan to take advantage of the ability of molecular dynamics to quantify the various activation barriers that we will then use for our kinetic Monte Carlo simulations.

- ¹U. Bardi, Rep. Prog. Phys. **57**, 939 (1994).
- ²A. Saúl, *Materials Science Forum* (Trans Tech, Aedermannsdorf, Switzerland, 1994) Vols. 155/156, p. 233; A. Saúl, B. Legrand, and G. Tréglia, Surf. Sci. **331-333**, 805 (1995).
- ³B. Aufray, H. Giordano, B. Legrand, and G. Tréglia, Surf. Sci. **307-309**, 531 (1994).
- ⁴A. Rolland and B. Aufray, Surf. Sci. **162**, 530 (1985).
- ⁵B. C. Bolding and E. A. Carter, Surf. Sci. **268**, 142 (1992).
- ⁶P. J. Schmitz, W. Y. Leung, G. W. Graham, and P. A. Thiel, Phys. Rev. B **40**, 11 477 (1989).
- ⁷S.-L. Chang, J.-M. Wen, P. A. Thiel, S. Günther, J. A. Meyer, and R. J. Behm, Phys. Rev. B **53**, 13 747 (1996).
- ⁸T. J. Raeker, D. E. Sanders, and A. E. DePristo, J. Vac. Sci. Technol. A **8**, 3531 (1990).
- ⁹D. Rouyer, C. Krembel, M. C. Hanf, D. Bolmont, and G. Gewinner, Surf. Sci. **287/288**, 935 (1993); C. Krembel, M. C. Hanf, J. C. Peruchetti, D. Bolmont, and G. Gewinner, J. Vac. Sci. Technol. A **10**, 3325 (1992).
- ¹⁰M. Canepa, E. Magnano, A. Campora, P. Cantini, M. Salvietti, and L. Mattered, Surf. Sci. **352**, 36 (1996); M. Canepa, M. Salvietti, A. Campora, and L. Mattered, J. Electron Spectrosc. Relat. Phenom. **76**, 471 (1995).
- ¹¹Li Hong and B. P. Tonner, Surf. Sci. **237**, 141 (1990).
- ¹²A. K. Schmid, D. Atlan, H. Itoh, B. Heinrich, T. Ichinokawa, and J. Kirschner, Phys. Rev. B **48**, 2855 (1993).
- ¹³Th. Detzel and N. Memmel, Phys. Rev. B **49**, 5599 (1994).
- ¹⁴W. F. Egelhoff, Jr., J. Vac. Sci. Technol. A **7**, 2060 (1989).
- ¹⁵M. I. Haftel, M. Rosen, T. Franklin, and M. Hettermann, Phys. Rev. B **53**, 8007 (1996).
- ¹⁶Y. L. He and G. C. Wang, Phys. Rev. Lett. **71**, 3834 (1993).
- ¹⁷G. Tréglia, B. Legrand, and F. Ducastelle, Europhys. Lett. **7**, 575 (1988).
- ¹⁸F. Ducastelle, B. Legrand, and G. Tréglia, Prog. Theor. Phys. Suppl. **101**, 159 (1990).
- ¹⁹A. Senhaji, G. Tréglia, B. Legrand, N. T. Barrett, C. Guillot, and B. Villette, Surf. Sci. **274**, 297 (1992).
- ²⁰A. Senhaji, G. Tréglia, J. Eugène, A. Khoutami, and B. Legrand, Surf. Sci. **287/288**, 371 (1993).
- ²¹D. Tománek, A. A. Aligia, and C. A. Balseiro, Phys. Rev. B **32**, 5051 (1985).
- ²²V. Rosato, M. Guillopé, and B. Legrand, Philos. Mag. A **59**, 321 (1989).
- ²³G. Tréglia and B. Legrand, Phys. Rev. B **35**, 4338 (1987).
- ²⁴G. Tréglia, B. Legrand, J. Eugène, B. Aufray, and F. Cabané, Phys. Rev. B **44**, 5842 (1991).
- ²⁵B. Legrand, A. Saúl, and G. Tréglia, *Materials Science Forum* (Trans Tech, Aedermannsdorf, Switzerland, 1994) Vols. 155/156, p. 165.
- ²⁶A. Saúl, B. Legrand, and G. Tréglia, Phys. Rev. B **50**, 1912 (1994).
- ²⁷N. Metropolis, A. W. Metropolis, M. N. Rosenbluth, A. H. Teller, and E. Teller, J. Chem. Phys. **21**, 1087 (1953).
- ²⁸G. Martin, Phys. Rev. B **41**, 2279 (1990).
- ²⁹J. Ladet, J. Bernardini, and F. Cabané-Brouty, Scr. Metall. **10**, 195 (1975).
- ³⁰J. M. Roussel, A. Saúl, G. Tréglia, and B. Legrand, Surf. Sci. **352-354**, 562 (1996).
- ³¹W. Romanowski, Surf. Sci. **18**, 373 (1969).
- ³²S. Valkealahti and M. Manninen, Phys. Rev. **50**, 17 564 (1994).
- ³³I. M. Lifshitz and V. V. Slyozov, J. Phys. Chem. Solids **19**, 35 (1961).
- ³⁴C. Wagner, Z. Electrochem. **65**, 581 (1961).
- ³⁵For a review on Ostwald ripening see, for example, J. W. Martin and R. D. Doherty, *Stability of Microstructure in Metallic Systems* (Cambridge University Press, London, 1976); J. S. Langer, in *Solids Far From Equilibrium* (Cambridge University Press, London, 1992), p. 297.
- ³⁶A. J. Ardell, Acta Metall. **20**, 61 (1972).
- ³⁷For a discussion between the surfactant effect in Ni/Ag and Au/Ag in terms of the energetic parameters of the TBIM, see Ref. 3.
- ³⁸C. T. Chan, K. P. Bohnen, and K. M. Ho, Phys. Rev. Lett. **69**, 1672 (1992).
- ³⁹S. Rousset, S. Chiang, D. E. Fowler, and D. D. Chambliss, Phys. Rev. Lett. **69**, 3200 (1992).
- ⁴⁰B. Aufray (private communication).
- ⁴¹Soon C. Hong, A. J. Freeman, and C. L. Fu, Phys. Rev. B **39**, 5719 (1989).